APPENDIX J

HZE Beam Transport in Multilayered Materials

by

J.L. Shinn, J.W. Wilson, F.F. Badavi, E.V. Benton
I. Csige, A.L. Frank and E.R. Benton

Pergamon

HZE BEAM TRANSPORT IN MULTILAYERED MATERIALS

J. L. Shinn,* J. W. Wilson,* F. F. Badavi,† E. V. Benton,‡ I. Csige,§ A. L. Frank‡
and E. R. Benton‡

*NASA Langley Research Center, Hampton, VA 23681, U.S.A.; †Christopher Newport University,
Newport News, VA 23601, U.S.A.; ‡University of San Francisco, San Francisco, CA 94117, U.S.A.;
and §Institute of Nuclear Research, ATOMKI, H-4001 Debrecen, Hungary

Abstract—A nonperturbative analytic solution of the high charge and energy (HZE) Green's function is used to implement a computer code for laboratory ion beam transport in multiple-layered materials. The code is established to operate on the Langley nuclear fragmentation model used in space engineering applications. Computational procedures are established to generate linear energy transfer (LET) distributions for a specified ion beam and target for comparison with experimental measurement. Comparison with ^{56}Fe ion with Pb–Al and Pb–$(CH_2)_x$ targets shows reasonable agreement.

1. INTRODUCTION

Green's functions were identified as the likely means of generating efficient HZE shielding codes for space engineering which are capable of being validated in laboratory experiments (Wilson *et al.*, 1989). A derivation of the Green's function as a perturbation series gave promise for development of a laboratory-validated engineering code (Wilson *et al.*, 1990) but computational inefficiency provided a major obstacle to code development (Wilson and Badavi, 1992). More recently, nonperturbative approximations to HZE Green's functions have shown promise in providing an efficient validated engineering code (Wilson *et al.*, 1993a, c). Previous work has found a solution to HZE transport in a homogeneous medium using nonperturbative methods (Wilson and Badavi, 1992; Wilson *et al.*, 1993b, c). In the present report, we derive solutions for inhomogeneous multi-layered media. The resulting computer code is used to derive LET spectra behind multilayered targets for ion beams with $Z \leqslant 28$ corresponding to the major components of the galactic cosmic ray spectrum. The results of the computation are compared with ^{56}Fe accelerator beam experiments with Pb–Al and Pb–$(CH_2)_x$ shield configurations.

2. GREEN'S FUNCTION FOR A SINGLE MEDIUM

We restrict our attention to the multiple charged ions for which the Boltzmann equation may be reduced (Wilson, 1977a) to:

$$\left[\frac{\partial}{\partial x} - \frac{\partial}{\partial E} \bar{S}_j(E) + \sigma_j\right] \phi_j(x, E) = \sum_k \sigma_{jk} \phi_k(x, E), \quad (1)$$

where $\phi_j(x, E)$ is the ion flux at x with energy E (MeV/amu), $\bar{S}_j(E)$ is the change in E per unit distance. σ_j the total macroscopic reaction cross section and σ_{jk} the macroscopic cross section for collision of ion type k to produce an ion of type j. The solution to equation (1) is to be found subject to the boundary condition:

$$\phi_j(0, E) = f_j(E), \quad (2)$$

which for laboratory beams has only one value of j for which $f_j(E)$ is not zero and that $f_j(E)$ is described by a mean energy E_0 and energy spread σ such that:

$$f_j(E) = \frac{1}{\sqrt{2\pi}\sigma} \exp[-(E - E_0)^2/2\sigma^2]. \quad (3)$$

The usual method of solution is to proceed solving equation (1) as a perturbation series (Wilson 1977a, b; Wilson *et al.*, 1990). In practice, the computational requirements limit the usefulness of the technique for deep penetration (Wilson and Badavi, 1992).

The Green's function is introduced as a solution of:

$$\left[\frac{\partial}{\partial x} - \frac{\partial}{\partial E} \bar{S}_j(E) + \sigma_j\right] G_{jm}(x, E, E_0)$$
$$= \sum_k \sigma_{jk} G_{km}(x, E, E_0), \quad (4)$$

subject to the boundary condition

$$G_{jm}(0, E, E_0) = \delta_{jm} \delta(E - E_0). \quad (5)$$

The solution to equation (1) is given by superposition as

$$\phi_j(x, E) = \sum_k \int G_{jk}(x, E, E') f_k(E') \, dE'. \quad (6)$$

If $G_{jk}(x, E, E')$ is known as a transcendental function, the evaluation of equation (6) may be accomplished by simple integration techniques, and the associated errors in numerically solving equation (1) are avoided (Wilson et al., 1991).

The above equations can be simplified by transforming the energy into the residual range as:

$$r_j = \int_0^E \mathrm{d}E'/\bar{S}_j(E'),\qquad(7)$$

and defining new field functions as:

$$\psi_j(x, r_j) = \bar{S}_j(E)\phi_j(x, E)\qquad(8)$$

$$\mathscr{G}_{jm}(x, r_j, r_m') = \bar{S}_j(E)G_{jm}(x, E, E')\qquad(9)$$

$$\hat{f}_j(r_j) = \bar{S}_j(E)f_j(E)\qquad(10)$$

and equation (4) becomes:

$$\left[\frac{\partial}{\partial x} - \frac{\partial}{\partial r_j} + \sigma_j\right]\mathscr{G}_{jm}(x, r_j, r_m')$$
$$= \sum_k \frac{v_j}{v_k}\sigma_{jk}\mathscr{G}_{km}(x, r_k, r_m'),\quad(11)$$

where v_j is the range scale factor as $v_j r_j = v_m r_m$ and is taken as $v_j = Z_j^2/A_j$ and the boundary condition is now:

$$\mathscr{G}_{jm}(0, r_j, r_m') = \delta_{jm}\delta(r_j - r_m')\qquad(12)$$

and with solution to the ion fields given by

$$\psi_j(x, r_j) = \sum_m \int_0^\infty \mathscr{G}_{jm}(x, r_j, r_m')\hat{f}_m(r_m')\,\mathrm{d}r_m'.\quad(13)$$

The solution to equation (11) is written as a perturbation series:

$$\mathscr{G}_{jm}(x, r_j, r_m') = \sum_i \mathscr{G}_{jm}^{(i)}(x, r_j, r_m')\qquad(14)$$

where

$$\mathscr{G}_{jm}^{(0)}(x, r_j, r_m') = g(j)\,\delta_{jm}\,\delta(x + r_j - r_m')\quad(15)$$

and

$$\mathscr{G}_{jm}^{(1)}(x, r_j, r_m') \approx \frac{v_j\sigma_{jm}g(j, m)}{x(v_m - v_j)}\qquad(16)$$

where $\mathscr{G}_{jm}^{(1)}(x, r_j, r_m')$ is zero unless

$$\frac{v_j}{v_m}(r_j + x) \leqslant r_m' \leqslant \frac{v_j}{v_m}r_j + x\qquad(17)$$

for $v_m > v_j$. If $v_j > v_m$, as can happen in neutron removal, the negative of equation (16) is used and the upper and lower limits of equation (17) are switched. The higher terms are approximated as:

$$\mathscr{G}_{jm}^{(i)}(x, r_j, r_m') \approx \sum_{k_1, k_2, \ldots, k_{i-1}}$$
$$\times \frac{v_j\sigma_{jk_1}\sigma_{k_1k_2}\cdots\sigma_{k_{i-1}m}g(j, k_1, k_2, \ldots, k_{i-1}, m)}{x(v_m - v_j)}.$$
$$(18)$$

In the above, the g-function of n-arguments is found recursively by:

$$g(j) = e^{-\sigma_j x}\qquad(19)$$

and

$$g(j_1, j_2 \cdots j_n, j_{n+1})$$
$$= \frac{g(j_1, j_2 \cdots j_{n-1}, j_n) - g(j_1, j_2 \cdots j_{n-1}, j_{n+1})}{\sigma_{j_{n+1}} + \sigma_{j_n}}.$$
$$(20)$$

Note that the $\mathscr{G}_{jm}^{(i)}(x, r_j, r_m')$ are purely dependent on x for $i > 0$ which we represent as $\mathscr{G}_{jm}^{(i)}(x)$ (Wilson and Badavi, 1992). In terms of the above, the solution to equation (1) becomes (Wilson and Badavi, 1992)

$$\psi_j(x, r_j) = e^{-\sigma_j x}\hat{f}_j(r_j + x)$$
$$+ \sum_{m,i}\mathscr{G}_{jm}^{(i)}(x)[\hat{F}_m(r_{ml}') - \hat{F}_m(r_{mu}')].\quad(21)$$

In equation (21), r_{mu}' and r_{ml}' are given by the upper and lower limits of the inequality (17). The symbol $\hat{F}_m(r_m')$ refers to the integral spectrum:

$$\hat{F}_m(r_m') = \int_{r_m'}^\infty \hat{f}_m(r)\,\mathrm{d}r.\qquad(22)$$

We note that:

$$\hat{F}_m(r_m') \equiv F_m(E')\qquad(23)$$

with

$$F_m(E') = \int_E^\infty f_m(E)\,\mathrm{d}E\qquad(24)$$

and

$$r_m' = \int_0^E \mathrm{d}E/\bar{S}_m(E).\qquad(25)$$

We now introduce nonperturbative terms for the summation in equation (21).

First, we recall that the g-function of n-arguments was generated by the perturbation solution of the transport equation neglecting ionization energy loss (Wilson et al., 1989) given by:

$$\left[\frac{\partial}{\partial x} + \sigma_j\right]g_{jm}(x) = \sum_k \sigma_{jk}g_{km}(x)\qquad(26)$$

subject to the boundary condition:

$$g_{jm}(0) = \delta_{jm}\qquad(27)$$

for which the solution is

$$g_{jm}(x) = \delta_{jm}g(m) + \sigma_{jm}g(j, m) + \cdots\qquad(28)$$

It is also true that:

$$g_{jm}(x) = \sum_k g_{jk}(x - y)g_{km}(y)\qquad(29)$$

for any positive values of x and y. Equation (29) may

be used to propagate the function $g_{jm}(x)$ over the solution space, after which:

$$\mathcal{G}_{jm}(x, r_j, r_m') \approx e^{-\sigma_j x} \delta_{jm} \delta(x + r_j - r_m')$$
$$+ v_j[g_{jm}(x) - e^{-\sigma_j x}\delta_{jm}]/x(v_m - v_j). \quad (30)$$

The approximate solution of equation (1) is then given by

$$\psi_j(x, r_j) = e^{-\sigma_j x/(r_j + x)}$$
$$+ \sum_m \frac{v_j[g_{jm}(x) - e^{-\sigma_j x}\delta_{jm}]}{x(v_m - v_j)}[\hat{F}_m(r_{mu}') - \hat{F}_m(r_{ml}')]$$
$$(31)$$

which is a relatively simple quantity (Wilson et al., 1993a).

3. GREEN'S FUNCTION IN A SHIELDED MEDIUM

The major simplification in the Green's function method results from the fact that the scaled spectral distribution of secondary ions to a first approximation depends only on the depth of penetration as seen in equations (16), (18) and (30). Our first approach to a multilayered Green's function will rely on this observation and assume its validity for multilayered shields.

Consider a domain labeled as 1 which is shielded by a second domain labeled as 2; the number of type j ions at depth x in 1 due to type m ions incident on domain 2 of thickness y is:

$$g_{12jm}(x, y) = \sum_k g_{1jk}(x)g_{2km}(y). \quad (32)$$

The leading term in equation (32) is the penetrating primaries as:

$$g_{12jm}(x, y) = e^{-\sigma_{1j}x - \sigma_{2j}y}\delta_{jm}$$
$$+ [g_{12jm}(x, y) - e^{-\sigma_{1j}x - \sigma_{2j}y}\delta_{jm}], \quad (33)$$

where all higher order terms are in the bracket of equation (33).

The first term of the scaled Green's function is then:

$$\mathcal{G}_{12jm}^{(0)}(x, y, r_j, r_m') = e^{-\sigma_{1j}x - \sigma_{2j}y}\delta_{jm}$$
$$\times \delta[x + r_j - (r_m' - \rho y)], \quad (34)$$

where ρ is the range factor for the two media:

$$\rho = R_{1j}(E)/R_{2j}(E). \quad (35)$$

The ratio is shown for protons in Fig. 1. We take a single value for ρ corresponding to 600 MeV/amu. The secondary contribution is similarly found by noting that equation (17) becomes:

$$\frac{v_j}{v_m}(r_j + x + \rho y) \leqslant r_m' \leqslant \frac{v_j}{v_m}r_j + x + \rho y, \quad (36)$$

from which the average spectrum is evaluated. The full approximate Green's function is then:

$$\mathcal{G}_{12jm}(x, y, r_j, r_m') \approx e^{-\sigma_{1j}x - \sigma_{2j}y}\delta_{jm}$$
$$\times \delta(x + \rho y + r_j - r_m') + v_j[g_{12jm}(x, y)$$
$$- e^{-\sigma_{1j}x - \sigma_{2j}y}\delta_{jm}]/(x + \rho y)(v_m - v_j). \quad (37)$$

Equation (37) is our first approximation to the Green's function in a shielded medium (two layers) and is easily modified to multiple layers (see Appendix). We now consider the first spectral modification.

It is easy to show that the first collision term has the properties:

$$\mathcal{G}_{12jm}^{(1)}(x, y, r_j, r_m')$$
$$= \begin{cases} \dfrac{v_j\sigma_{1jm}e^{-\sigma_{1m}x - \sigma_{2m}y}}{|v_m - v_j|} & \text{for } r_m' = r_{mu}' \\[2ex] \dfrac{v_j\sigma_{2jm}e^{-\sigma_{1j}x - \sigma_{2j}y}}{|v_m - v_j|} & \text{for } r_m' = r_{ml}'. \end{cases} \quad (38)$$

We use these properties to correct the average spectrum as:

$$\mathcal{G}_{12jm}^{(1)}(x, y, r_j, r_m') = \frac{v_j g_{12jm}^{(1)}(x, y)}{|v_m - v_j|(x + \rho y)}$$
$$+ b_{jm}(x, y)(r_m' - \bar{r}_m), \quad (39)$$

where $g_{12jm}^{(1)}(x, y)$ is the first collision term of equation (37) and

$$\bar{r}_m' = (r_{mu}' + r_{ml}')/2 \quad (40)$$

is the midpoint of $\bar{r}_m'$ between its limits given by equation (36). The b_{jm} term of equation (39) has the property that:

$$\int_{r_{ml}'}^{r_{mu}'} b_{jm}(x, y)(r' - \bar{r}_m') \, dr' = 0, \quad (41)$$

ensuring that the first term of equation (39) is indeed the average spectrum as required. The spectral slope parameter is found to be:

$$b_{jm}(x, y) = v_j v_m(\sigma_{1jm}e^{-\sigma_{1m}x - \sigma_{2m}y} - \sigma_{2jm}$$
$$\times e^{-\sigma_{1j}x - \sigma_{2j}y})/[(x + \rho y)(v_m - v_j)|v_m - v_j|]. \quad (42)$$

A similarly simple spectral correction could be made to the higher order terms. The spectral correction given in equation (42) is included in the present Green's function code.
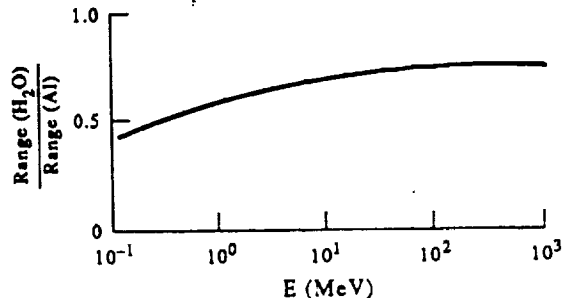

FIG. 1. Ratio of range in water to range in aluminum for proton beams.

4. LET SPECTRA FOR LABORATORY BEAMS

We use the boundary condition appropriate for laboratory beams given by equation (3). The cumulative spectrum is given by:

$$F_j(E) = \frac{1}{2}\left[1 - erf\left(\frac{E - E_0}{\sqrt{2}\sigma}\right)\right].\quad (43)$$

The cumulative energy moment needed to evaluate the spectral correction is:

$$E_j(E) = \frac{1}{2}E_0\left[1 - erf\left(\frac{E - E_0}{\sqrt{2}\sigma}\right)\right]$$
$$+ \frac{\sigma}{\sqrt{2\pi}}\exp\left[-\frac{(E - E_0)^2}{2\sigma^2}\right].\quad (44)$$

The average energy on any subinterval (E_1, E_2) is then:

$$\bar{E} = [E_j(E_1) - E_j(E_2)]/[F_j(E_1) - F_j(E_2)].\quad (45)$$

The beam generated flux is:

$$\psi_j(x, y, r_j) = e^{-\sigma_{1j}x - \sigma_{2j}y}\hat{f}_j(r_j + x + \rho y)$$
$$+ \sum_{m,i}\mathcal{G}_{jm}^{(i)}(x, y)[\hat{F}_m(r'_{mu}) - \hat{F}_m(r'_{mi})]$$
$$+ \sum_m b_{jm}^{(i)}(x, y)[r'_m(\bar{E}) - \bar{r}'_m]$$
$$\times [\hat{F}_m(r'_{mu}) - \hat{F}_m(r'_{mi})],\quad (46)$$

where $\bar{E}$ is evaluated using equation (45) with E_1, and E_2 as the lower and upper limits associated with r'_{mi} and r'_{mu}.

A series of evaluations for a lead scattering foil (2.24 g/cm²) in front of a water target is shown in Fig. 2. The lead scattering foil is usually part of the accelerator beam line so that the fragments from the
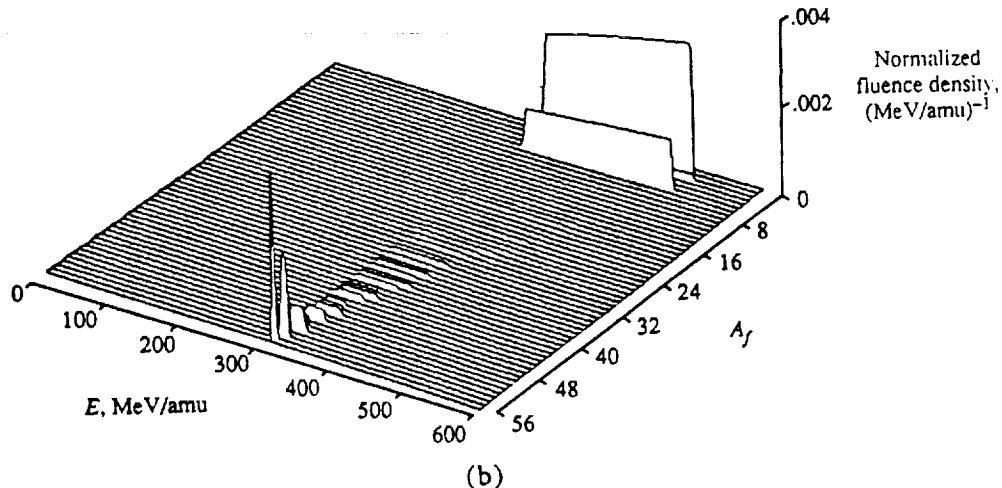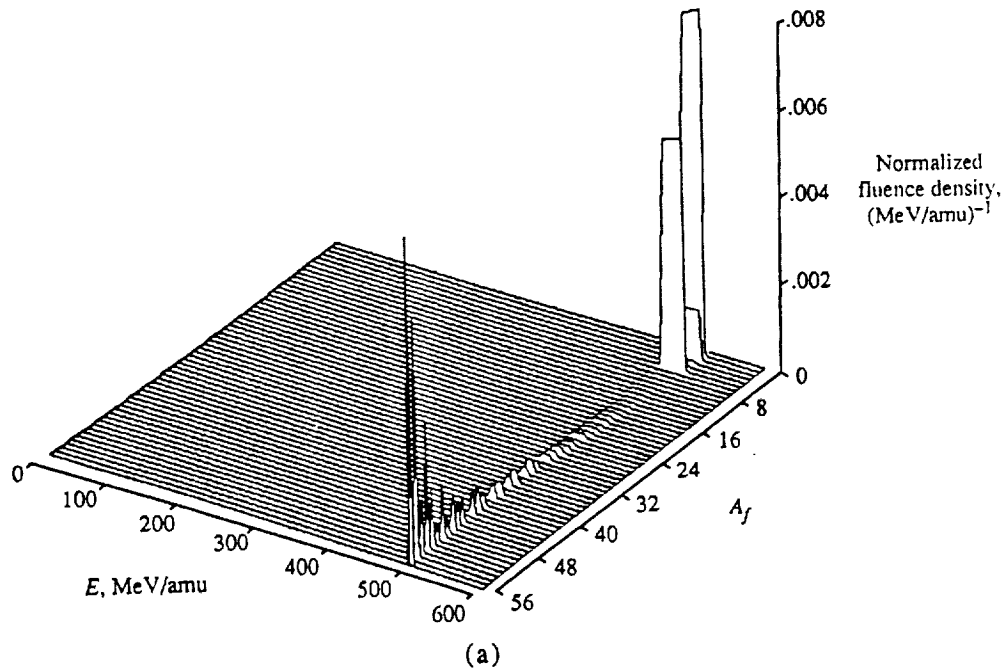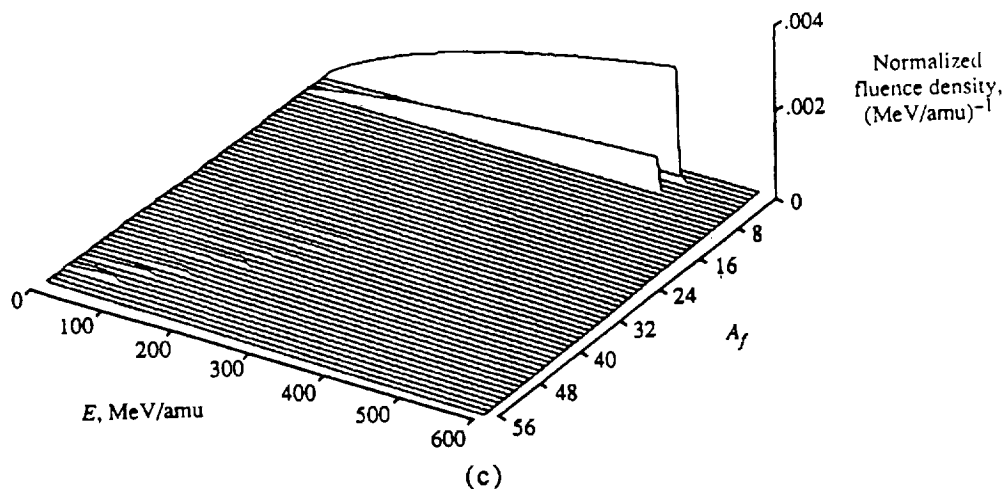

(a)

(b)

Fig. 2 (a) and (b).

Fig. 2. Differential fluence for 525 MeV/amu ^{56}Fe beam with a 2.5 MeV/amu standard deviation after passing through a 2.24 g/cm^2 lead scattering foil and a water target. (a) 0 cm H$_2$O; (b) 5 cm H$_2$O; (c) 10 cm H$_2$O.

lead target are seen as contamination. Clearly, these fragments must be modeled to properly interpret the attenuation of the beam in the water target in actual experiments.

5. NUCLEAR DATA BASE

The nuclear absorption cross sections are fits to quantum mechanical calculations developed at the Langley Research Center over the past 20 years (Wilson, 1973, 1974; Wilson and Costner, 1975; Wilson and Townsend, 1981; Townsend and Wilson, 1986) and are considered reliable to about 10%. The nuclear fragmentation cross sections for most nuclei on hydrogen targets are taken from Silberberg et al. (1983) and are augmented for light fragment production with the Bertini model (Bertini, 1969). It was noted that early versions of these cross sections failed to conserve mass and charge (Wilson et al.,

1974) and still exhibit mass loss for $10 \leqslant Z \leqslant 22$ by as much as 30%. This is displayed in Fig. 3 where σ_{abs} is compared to $\Sigma A_i \sigma_{ip}/A_p$, where A_i is fragment mass, σ_{ip} is the fragmentation cross section for projectile p and A_p is the projectile mass. The breakup of light nuclei ($A \leqslant 4$) is taken from the quantum calculations of Cucinotta et al. (1993). The fragmentation of the remaining nuclei ($A_p > 4$) is evaluated from the latest versions of the NUCFRAG model (Wilson et al. 1987a, b). Since the public release version of NUCFRAG (HZE-FRG1, Townsend et al., 1993), a de-excitation scheme for mass two and mass three fragments and a coulomb trajectory calculation have been added for more realistic cross sections at low energy (Wilson et al., 1993a). The elemental fragmentation cross sections are displayed in Fig. 4 at several energies. The reduced light fragment production at low energy results from coulomb trajectory corrections. This is the same data base used in the most recent energy dependent engineering code HZETRN (Shinn et al., 1992).
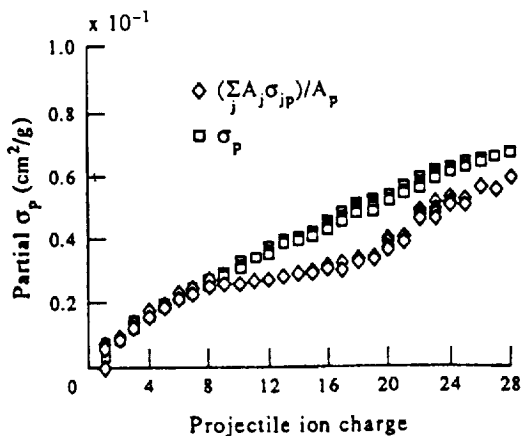
The transport codes usually represent a reduced set of isotopes. In the past, we usually represented each charge group with an associated mass taken as the nearest mass on the stability curve for the given fragment charge. The most recent version of HZETRN uses an isobaric flux representation with the nearest charge on the stability curve and the distance to the nearest isobar was calculated

$$D = (A_i - A_l)^2 + 4(Z_i - Z_l)^2, \qquad (47)$$

where A_i, Z_i represent the fragment and A_l, Z_l represent the listed isobar mass used in the calculation and nearest charge to the stability curve. The present calculation uses an 80-isotope representation and the nearest isotope in the list is found using equation (47).
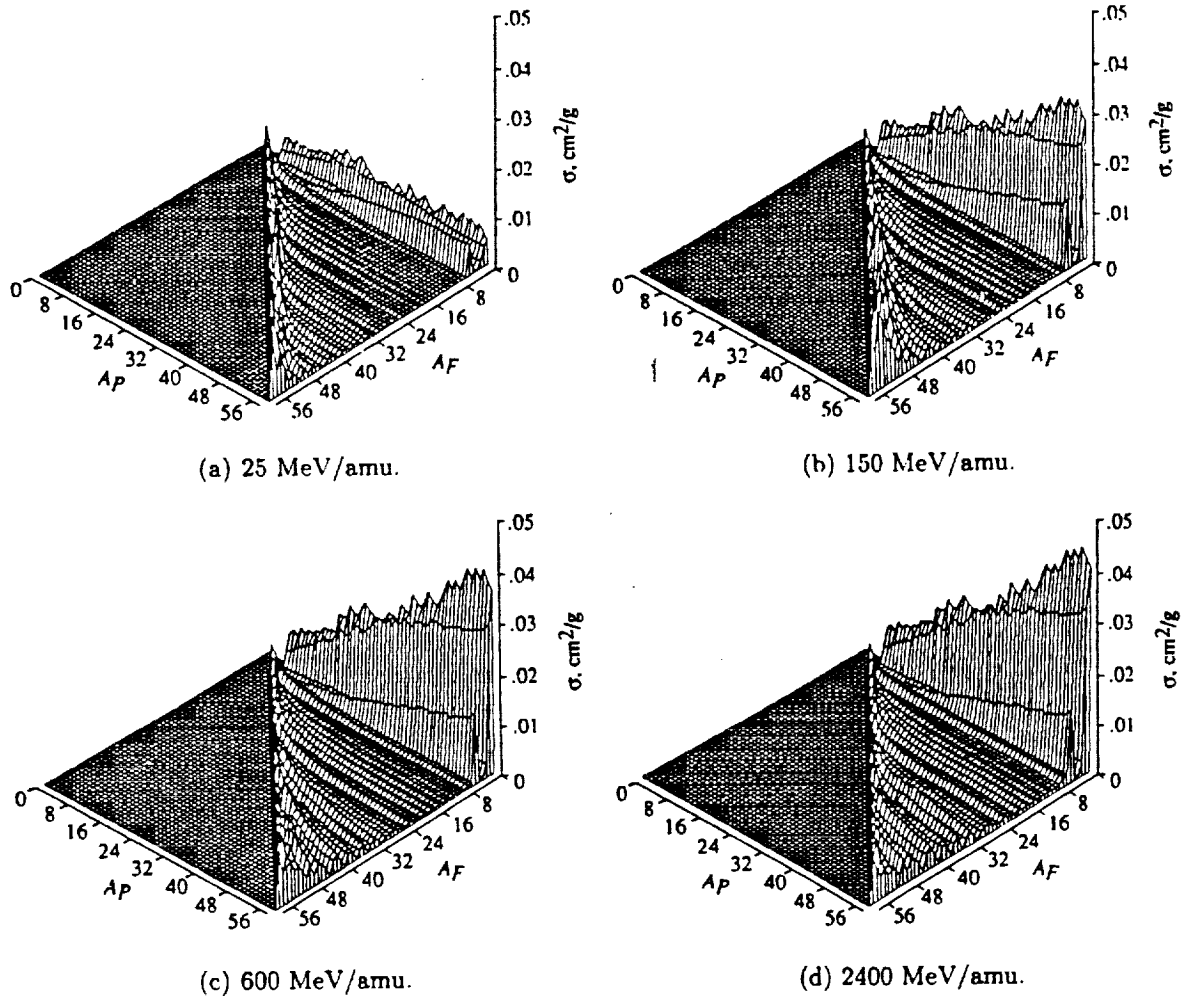

FIG. 3. The absorption cross section in hydrogen targets and mass averaged production cross sections at 600 MeV/amu for various projectiles.

(a) 25 MeV/amu.

(b) 150 MeV/amu.

(c) 600 MeV/amu.

(d) 2400 MeV/amu.

FIG. 4. The fragment production cross section in H_2O targets including coulomb corrections.

6. EXPERIMENTAL METHODS AND COMPARISON

The ^{56}Fe nuclei were accelerated to 600 MeV/amu at the Lawrence Berkeley Laboratory Bevalac facility and passed through a series of beam transport
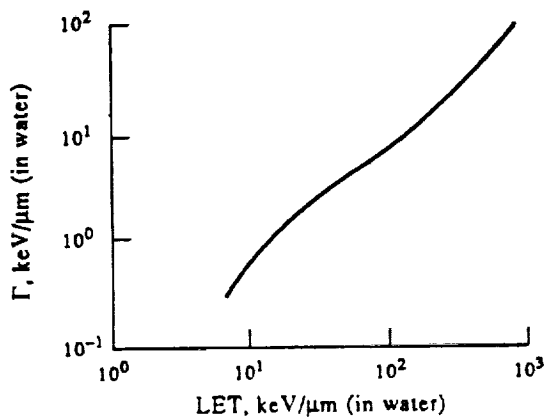

FIG. 5. Measured CR-39 response parameter (Benton *et al.*, 1986).

elements, triggering devices and a 2.24 g/cm^2 lead foil prior to exiting the beam pipe and impacting the target. Two targets of 2 g/cm^2 Al and 4.6 g/cm^2 of polyethylene $(CH_2)_x$ were used to evaluate their transport properties. The beam energy is inferred to be 557 MeV/amu when only the lead foil and target are considered for transport analysis. The transported beam exciting the target was measured using CR-39 plastic foils (Benton *et al.*, 1986). The beam intensity was measured by a monitoring foil in front of the target. The detectors and targets are run in good geometry so that acceptance corrections are not required.

The detector response is assumed to be approximately Gaussian with an LET dependent width Γ shown in Fig. 5. A correction for non-Gaussian contributions is taken as:

$$R(L, L_0) = 0.8 \frac{1}{\sqrt{2\pi\sigma_0^2}} e^{-(L - L_0)^2/2\sigma_0^2}$$

$$+ 0.2 \frac{1}{\sqrt{2\pi\sigma_1^2}} e^{-(L - L_0)^2/2\sigma_1^2}, \quad (48)$$

where $\sigma_0 = 0.4247\Gamma$ and σ_1 (taken as $2.4\sigma_0$) is fit to the
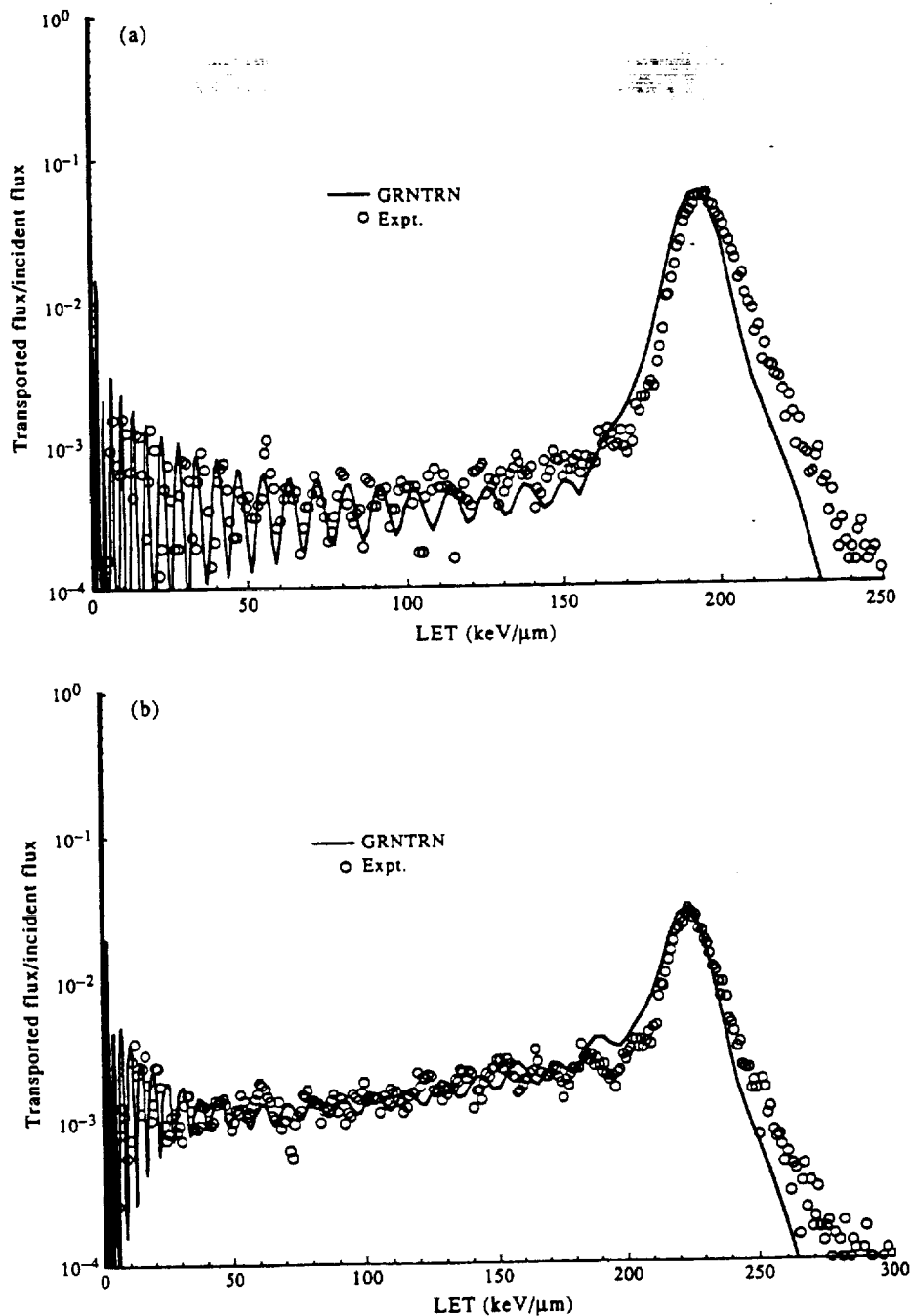
153

FIG. 6. Transport experiments for a lead-shield multilayer combination for 557 MeV/amu iron beams.
(a) 2.24 g/cm^2 Pb + 2 g/cm^2 Al; (b) 2.24 g/cm^2 Pb + 4.6 g/cm^2 (CH$_2$)$_x$.

high LET side of the primary ion peak. The response function of equation (48) is used to compare the theory to the experiment.

The distribution of ions produced in passing a 557 MeV/amu ^{56}Fe beam through a 2.24 g/cm^2 of lead and the two target materials (separately) was mapped into detector response using equation (48). The comparison with experimental measurements is shown in Fig. 6. While the calculated result for polyethylene is in good agreement with the experimental data (Fig. 6(b)), the calculated aluminum curve (Fig. 6(a)) suggests that the aluminum fragmentation cross sections may be 20–30% low.

REFERENCES

Benton E. V., Ogura K., Frank A. L., Atallah T. and Rowe V. (1986) Response of different types of CR-39 to energetic ions, *Nucl. Tracks Radiat. Meas.* **12**, 79–82.

Bertini H. W. (1969) Intranuclear-cascade calculation of the secondary nucleon spectrum from nucleon–nucleus interactions in the energy range 340 to 2900 MeV and comparisons with experiments. *Phys. Rev.* **188**, 1711–1730.

Cucinotta F. A., Townsend L. W. and Wilson J. W. (1983) Description of alpha–nucleus interaction cross sections for cosmic ray shielding studies. NASA TP-3285.

Shinn J. L., John S., Tripathi R. K., Wilson J. W., Townsend L. W. and Norbury J. W. (1992) Fully energy-dependent HZETRN (a galactic cosmic-ray transport code). NASA TP-3243.

Silberberg R., Tsao C. H. and Letaw J. R. (1983) Improvement of calculations of cross sections and cosmic ray propagation. In *Composition and Origin of Cosmic Rays* (ed. Shapiro M. M.), pp. 321–336. D. Reidel Publ.

Townsend L. W. and Wilson J. W. (1986) Energy-dependent parameterization of heavy-ion absorption cross sections. *Radiat. Res.* **106**, 283–287.

Townsend L. W., Wilson J. W., Tripathi R. K., Norbury J. W., Badavi F. F. and Khan F. (1993) HZEFRG1: An energy-dependent semiempirical nuclear fragmentation model, NASA TP-3310.

Wilson J. W. (1973) Intermediate energy nucleon–deuteron elastic scattering. *Nucl. Phys.* **B66**, 221–224.

Wilson J. W. (1974) Multiple scattering of heavy ions, Glauber theory, and optical model. *Phys. Lett.* **B52**, 149–152.

Wilson J. W. (1977a) Analysis of the theory of high-energy ion transport. NASA TN D-8381.

Wilson J. W. (1977b) Depth–dose relations for heavy ion beams. *Virginia J. Sci.* **28**, 136–138.

Wilson J. W. and Badavi F. F. (1992) New directions in heavy ion shielding. *Proc. Topical Meeting on New Horizons in Radiation Protection and Shielding.* Am. Nuc. Soc. pp. 205–211.

Wilson J. W., Badavi F. F., Costen R. C. and Shinn J. L. (1993a) Nonperturbative methods in HZE transport. NASA TP-3363.

Wilson J. W., Chun S. Y., Badavi F. F. and John S. (1993b) Coulomb effects in low-energy nuclear fragmentation. NASA TP-3352.

Wilson J. W., Costen R. C., Shinn J. L. and Badavi F. F. (1993c) Green's function methods in heavy ion shielding. NASA TP-3311.

Wilson J. W. and Costner C. M. (1975) Nucleon and heavy ion total and absorption cross sections for selected nuclei. NASA TN D-8107.

Wilson J. W., Lamkin S. L., Farhat H., Ganapol B. D. and Townsend L. W. (1989) A hierarchy of transport approximations for high energy heavy (HZE) ions. NASA TM-4118.

Wilson J. W. and Townsend L. W. (1981) An optical model for composite nuclear scattering. *Can. J. Phys.* **59**, 1569–1576.

Wilson J. W., Townsend L. W. and Badavi F. F. (1987a) Galactic HZE propagation through the earth's atmosphere. *Radiat. Res.* **109**, 173–183.

Wilson J. W., Townsend L. W. and Badavi F. F. (1987b) A semiempirical nuclear fragmentation model. *Nucl. Inst. Meth. Phys. Res.* **B18**, 225–231.

Wilson J. W., Townsend L. W., Bidasaria H. B., Schimmerling W., Wong M. and Howard J. (1984) ^{20}Ne depth–dose relations in water. *Health Phys.* **46**, 1101–1111.

Wilson J. W., Townsend L. W., Lamkin S. L. and Ganapol B. D. (1990) A closed form solution to HZE propagation. *Radiat. Res.* **122**, 233–228.

Wilson J. W., Townsend L. W., Schimmerling W., Khandelwal G. S., Khan F., Nealy J. E., Cucinotta F. A., Simonsen L. C., Shinn J. L. and Norbury J. W. (1991) Transport methods and interactions for space radiations. NASA RP-1257.

APPENDIX

The preceding formalism is extended to a three-layer configuration as follows. The solution to equation (26) in a three-layered medium is:

$$g_{123,jm}(x, y, z) = \sum_{kl} g_{1,jk}(x) g_{2kl}(y) g_{3lm}(z). \quad (A1)$$

The leading term is the penetrating primaries, and equation (A1) may be written as:

$$g_{123,jm}(x, y, z) = e^{-\sigma_{1j}x - \sigma_{2j}y - \sigma_{3j}z} \delta_{jm}$$
$$+ [g_{123,jm}(x, y, z) - e^{-\sigma_{1j}x - \sigma_{2j}y - \sigma_{3j}z} \delta_{jm}]. \quad (A2)$$

The scaled Green's function is then:

$$\mathcal{G}_{123,jm}(x, y, z, r_j, r_m') \approx - e^{-\sigma_{1j}x - \sigma_{2j}y - \sigma_{3j}z} \delta_{jm}$$
$$\times \delta(x + \rho_2 y + \rho_3 z + r_j - r_m') + v_j [g_{123,jm}(x, y, z)$$
$$- e^{-\sigma_{1j}x - \sigma_{2j}y - \sigma_{3j}z} \delta_{jm}]/(x + \rho_2 y + \rho_3 z)(r_m - r_j),$$
$$(A3)$$

where $\rho_2 = R_{1j}(E)/R_{2j}(E)$ and $\rho_3 = R_{1j}(E)/R_{3j}(E)$. The range condition of equation (17) becomes:

$$\frac{v_j}{v_m}(r_j + x + \rho_2 y + \rho_3 z) \leqslant r_m' \leqslant \frac{v_j}{v_m} r_j + x + \rho_2 + \rho_3 z. \quad (A4)$$

The spectral corrections are similarly derived.